Journal of New Technology and Materials
JNTM
Vol. 07, N°01 (2017)47-52

OEB Univ. Publish. Co.

The heterostructure ZnO/Al/SiO2/Si fabrication for Piezoelectric SAW and BAW Transducers and Sensors

R. Serhane [a], F. Hadj-Larbi [a], S. Lafane [b], S. Abdelli-Messaci [b] and T. Boutkedjirt [c]

[a] *Division Microélectronique et Nanotechnologie, Centre de Développement des Technologies Avancées (CDTA). Cité 20 Août 1956, Baba Hassen, BP: 17, DZ-16303, Algiers Algeria, E-mail : rafik_serhane@hotmail.com*

[b] *Division Milieux Ionisés et Laser, Centre de Développement des Technologies Avancées (CDTA). 20 Août 1956, Baba Hassen, BP: 17, DZ-16303, Algiers, Algeria.*

[c] *Equipe de Recherche Physique des Ultrasons, Faculté de Physique, Université des Sciences et de la Technologie Houari Boumediene (USTHB), BP 32, El-Alia, Bab-Ezzouar, DZ-16111 Algiers, Algeria.*

Corresponding author: email: rafik_serhane@hotmail.com, rserhane@cdta.dz

Received date: March 23, 2017; revised date: May 11, 2017; accepted date: May 23, 2017

Abstract

Zinc oxide (ZnO) thin films were deposited by pulsed laser deposition technique for making ZnO/Al/SiO_2/Si Bulk and Surface Acoustic Wave (BAW and SAW) transducers. The aim is to improve the piezoelectric properties of the ZnO films, which are strongly linked to their texture and microstructure. ZnO films with a wurtzite structure were deposited on the Al electrode layer, at different substrate temperatures, within the 100-500°C range. The characterization by X-ray diffraction showed that the deposited Al electrode was (111) oriented and that the ZnO film has a c-axis (002) preferential orientation. The scanning electron microscopy of the ZnO films on Al/SiO_2/Si substrate showed an evidence of compact grains with a honeycomb-like structure on surface and a columnar structure on cross-section appeared after a sequential transition of amorphous to non-oriented to crystalline phase. The results indicated that the optimum substrate temperature is of 300°C and the electrical input impedance measurement on the Al/ZnO/Al BAW structure showed a piezoelectric response, where the fundamental resonance mode was located at 160 MHz, with an electromechanical coupling coefficient K_{eff}^2 equal to 3.2%. The best piezoelectric response is obtained at the fourth (4th) thickness mode vibration, located at the frequency of 636.3 MHz and having K_{eff}^2 of 9.10%.

Keywords: ZnO, Pulsed laser deposition, Piezoelectricity, BAW and SAW, Thin films ;

1. Introduction

In the past 10 years, Zinc oxide (ZnO) become a very popular material for its large use in thin films [1]. Due to its physical properties of semiconductor, electromechanical transducer and nanocrystalline thin film [2], ZnO has a potential application as schottky diode and solar cell application [3], It is alsoo very interesting for several Micro and Nano-Electro Mechanical Systems (MEMS [4] and NEMS [5]) applications. The high electromechanical coupling coefficient makes ZnO extremely promising as a piezoelectric element for sensors and actuators [6] and for many piezoelectric applications like Surface Acoustic Wave (SAW) [7] and Bulk Acoustic Wave (BAW) [8] transducers. ZnO thin films can be fabricated using phase Spray pyrolysis [9] sol-gel process [10], RF magnetron sputtering [11] and laser ablation [12-14], etc.

In this work, a polycrystalline ZnO was prepared by the Pulsed Laser Deposition (PLD) technique, at different substrate temperatures, ranging from 100 to 500 °C, on multilayer Al(111)/SiO_2/Si substrate. The Al film (with a thickness of 250 nm) considered as the bottom electrode for BAW transducers was prepared, by Electron Beam Evaporation (EBE) technique and deposited, at room temperature, on a 2µm-SiO_2 layer. The SiO_2 film was performed by Silicon wet oxidation step. The BAW transducer was used to study the piezoelectric properties of the deposited ZnO, which could be used in transducers and sensors applications, or

2. Experimental procedures

2.1. Thermal Oxidation of Silicon

The electrical isolation of the device from the Si (100) p-type substrate was performed by using an intermediate SiO_2 layer, this former was grown by a thermal oxidation step of Silicon, according to a dry-wet-dry process, as follows:

- **Furnace load step:** from T=800 °C to 1100 °C, with a heating rate of 5 °C/min, under a gas flow of O_2=500 sccm and N_2=6000 sccm.
- **Dry oxidation step: during t=10 min at T=1100 °C, with O_2=6000 sccm.**
- **Wet oxidation step:** during t=9h 10 min at T=1100°C, under a mixture of (H_2+O_2)(5+3.5) slm.
- **Dry oxidation step:** during t=10 min at T=1100 °C, with an O_2 flow of 6000 sccm.
- **Furnace unload step** : from T=1100 °C to 800 °C, with a rate of 5 °C/min, under an O_2 gas flow of 500 sccm and a N_2 flow of 6000 sccm.

The temperature cycle is presented in (Fig 1.a) and the SEM micrograph of the obtained 2 µm-SiO_2 film was shown in (Fig 1.b).

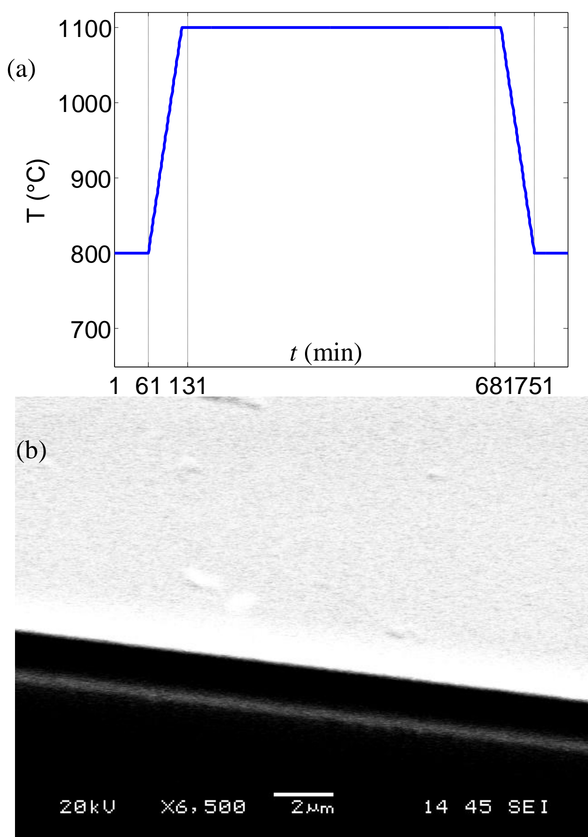

Fig. 1: (a)-Oxidation cycle, (b)- SEM characterization of the SiO_2 film obtained by the thermal oxidation.

2.2. . Deposition of the Al electrode on SiO_2 by EBE technique

The Al buffer layer, which serves as a bottom electrode for the piezoelectric characterization, has been deposited by the Electron Beam Evaporation (EBE) technique on the SiO_2 layer. The deposition is realized during 35 min at a pressure of 1.6 10^{-6} mbar with a current intensity of 0.486 A and a voltage of 6.17 kV. The deposition rate is estimated to be 1.2 Å/s.

2.2.1. Surface morphology and cristallinity of the Al thin film

The surface morphology of the Al grown films (Fig.2.a) is analyzed by a SEM (SEM-JEOL 6400) and the Al films microstructure (Fig 2.b) is determined with a Bruker D8 X-ray diffractometer (Advance (θ,2θ), Cu Kα and λ_0=1.5406 Å) in a grazing incidence. Figure 2.a shows that the Al thin film is uniformly deposited on the SiO_2 surface, its surface is smooth and no cracks are observed. The X-Ray Diffraction (XRD) patterns of Al thin films grown on a SiO_2/Si substrate (Fig 2.b) showed that the Al has different crystalline orientations ([111], [200], [220] and [311]), but if, in addition, we take into account the K_β X-ray radiation, the [111] direction becomes the most predominant orientation.

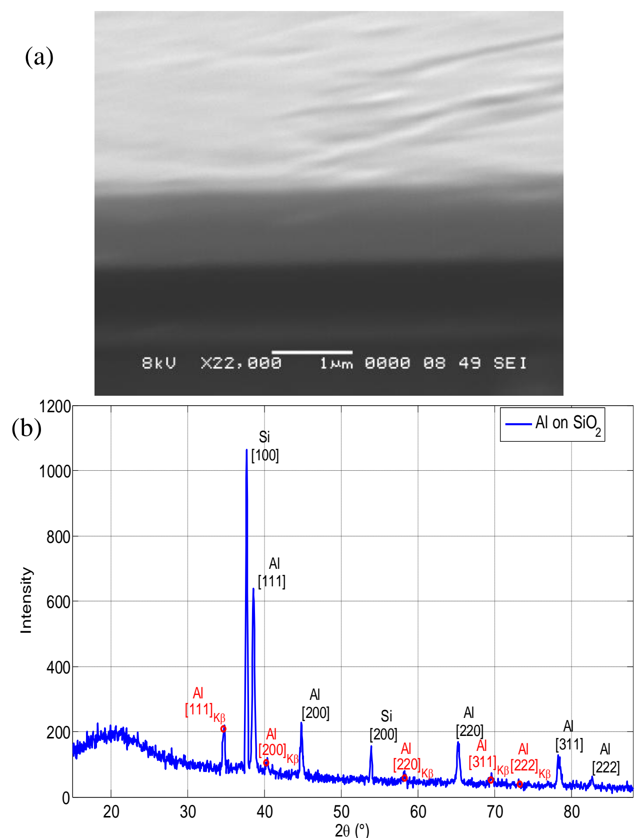

Fig. 2: Characterization of the Al thin film deposited on the SiO_2/Si substrate, (a)-SEM image of the Al layer and (b)- XRD patterns obtained at a grazing incidence.

2.3. Elaboration of the ZnO thin films by PLD

The Al/SiO_2/Si substrate of 0.25µm/2µm/350µm thickness respectively is mechanically attached to a heating block in a PLD chamber at vacuum of 10^{-6} mbar. A power generator monitors the temperature of the substrate. The ZnO target is fixed on the rotated holder located at 4 cm

far from the substrate holder. The pulsed KrF laser beam, (f=10 Hz, λ=248 nm and τ=25 ns), is directed at 45° with respect to its normal and focused on the target surface at a fluence of 2 J/cm^2. The vacuum chamber is, then, filled with Oxygen until obtaining the pressure of 10^{-2} mbar [15]. The deposition of ZnO is performed during 1h30min at the substrate temperatures of 100, 200, 300, 400 and 500°C.

3. Results and discussion

3.1. ZnO this film characterization

3.1.1. Crystallinity of the ZnO thin films

Fig. 3.a shows the XRD patterns of the ZnO thin films deposited on Al at different substrate temperatures (T_s), the ZnO polycrystalline film of Wurtzite structure grows in a preferred (002) orientation (located at 2θ=34.48°) corresponding to the P6$_3$*mc* space group [16]. We notice that the ZnO thin film structure is sensitive to the deposition substrate temperature. Indeed, for all the obtained diffractograms, from 100 to 500 °C, the film realized at 300 °C exhibits the strongest intensity of the (002) peak of diffraction.

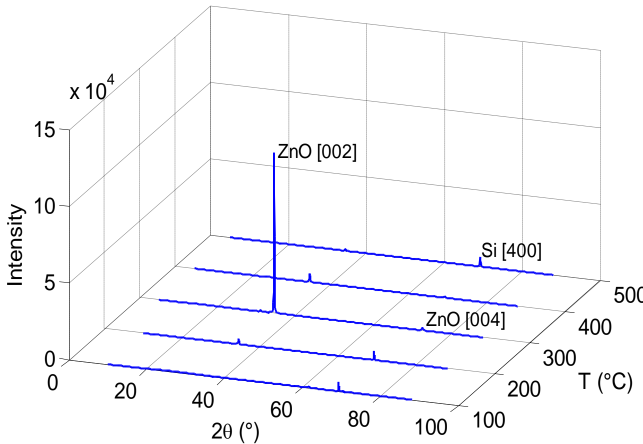

Fig. 3: a)- XRD patterns of the elaborated ZnO at different substrate temperatures

To assess the crystallite grain size D (coherence length) of the ZnO films, the line breadth β is calculated by fitting the (002) ZnO peak at 34.48° (observed in Fig.3.a) with the pseudo-Voigt function and taking the corresponding full width at half maximum. The line breadth β is related to the grain size D according to Scherrer formula [17, 18]:

$$D=\frac{0.9\lambda_0}{\beta.\cos(\theta_0)}, \quad (1)$$

where λ_0=1.5406 Å is the Cu-K$_\alpha$ radiation wavelength and θ_0 the Bragg angle corresponding to the (002) ZnO peak. The line breadth value is around 0.18° for the ZnO at 300 °C. The grain size is evaluated to 47 nm, which means a high quality of the ZnO films elaborated by PLD [19]. The c_0 lattice constant of the ZnO hexagonal unit cell is calculated from the Bragg relationship using $1/d_{hkl}^2=4(h^2+hk+k^2)/3a_0^2+l^2/c_0^2$ [20] (h=0, k=0, l=2), where c_0 is close to 5.207 Å [21].

3.1.2. Surface morphology characterization of the ZnO thin film

Fig. (4) shows the SEM images of the ZnO thin film deposited on Al/SiO$_2$/Si at 300°C. The surface morphology of the ZnO film on Al (Fig. 4.a) presents some roughness and shows a macroporous structure of a honeycomb-type morphology. The SEM cross-section image (see Figure (4.b)) shows a compact structure of the ZnO thin film and a columnar grain growth along the c-axis. The crystallized grains are perpendicular to the substrate surface, and this is a consequence of the high growth rate (~1.24 Å/pulse) of ZnO along the c-axis [22] which also promotes the growth of (002) polar planes with the lowest surface free energy [23]. This plane is formed by the creation of an electronegative surface caused by the Oxygen plane, the polar plane increases the flux of incident species by attracting the Zn$^+$ species and depositing an electropositive Zinc plane, and so on. This mechanism leads to the formation of alternate planes of Zn atoms and O atoms [24], forming a hexagonal (Wurtzite) structure.

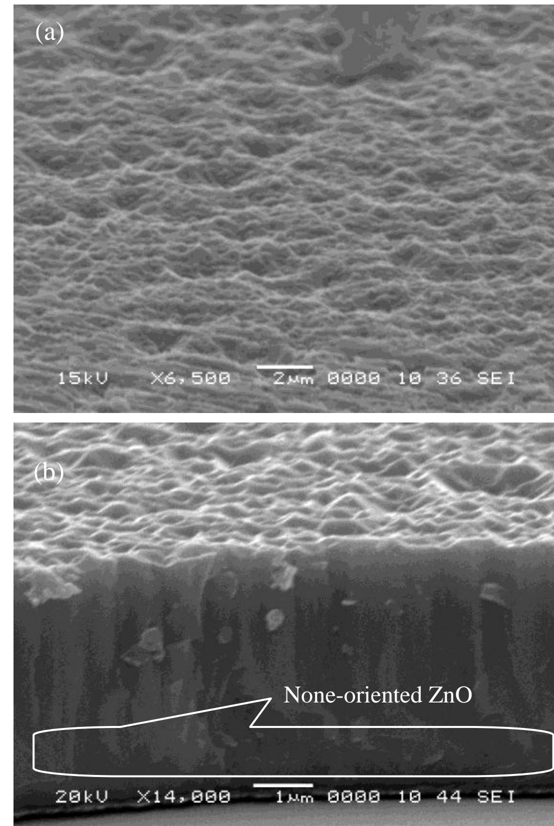

Fig.4: Characterization of the ZnO thin films deposited on Al/SiO$_2$/Si substrate; (a)- SEM surface morphology of sample realized at 300°C and (b)- SEM cross-section.

The ZnO film presents a stratified structure with continuous transitions between each other. A first layer is constituted of an amorphous phase of ZnO, followed by a non-oriented layer, and finally comes the oriented layer of ZnO (see Fig. 4.b). The amorphous phase of ZnO is due to an amorphous Aluminum oxide layer, which is formed on the Aluminum electrode surface by injecting Oxygen in the PLD chamber. This oxidation occurs during the time in which the Oxygen pressure is stabilized and the substrate is heated at 300 °C (roughly 10 to 15min before the ablation process).

In order to study the evolution of (002) ZnO peak in function of the thickness (grown on $Al/SiO_2/Si$ substrate), we have done a set of XRD measurements on samples realized at different deposition times (7, 15, 30 and 45 min) corresponding to different thicknesses (~0.26, 0.56, 1.12 and 1.68 µm, respectively). These XRD data are presented in the figure (5.a), where the well-oriented (002) ZnO becomes clearly visible beyond 30 min of deposition time, and this corresponds approximately to 1µm thickness. For the first 7 minutes of deposition, no orientation of ZnO is observed; so, we assume that at this stage, the ZnO has an amorphous phase, and then, at 15 min, some phases become weakly apparent. At 30 min and beyond, the (002) peak is the predominant phase.

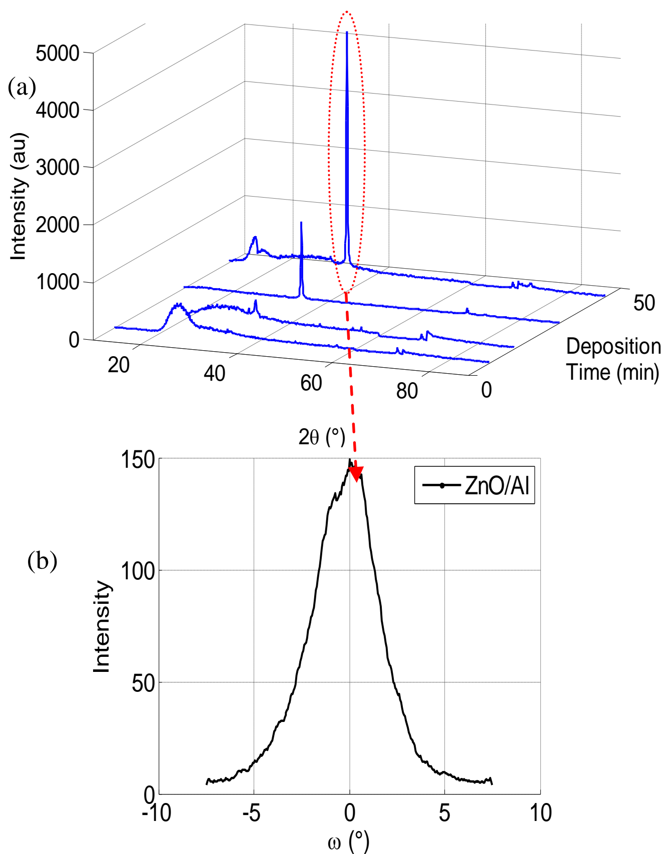

Fig. 5: (a)- XRD characterization of ZnO on Al for different deposition times (7, 15, 30 and 45 minutes) and (b)- XRD rocking curve of (002) c-axis of ZnO/Al deposited at 300°C.

The crystalline quality (mosaicity) of the elaborated ZnO thin film is evaluated by the rocking curve measurements [25] on the (002) diffraction peaks (Fig. 5.b), carried out for the sample of ZnO deposited at 300 °C during 90 minutes. This measurement permits to evaluate the degree of the *c*-axis alignment with respect to the normal of the substrate. The FWHM (Full Width at Half Maximum) value of this rocking curve is 3.75°, which means a good crystalline quality of the ZnO deposited on Al.

3.2. Deposition of the Al top electrode by thermal evaporation

In order to evaluate the piezoelectric effect of the considered BAW transducer ($Al/ZnO/Al/SiO_2/Si$ structure), a circular top electrode (with a radius of 1.8 mm) is made on the ZnO surface by a thermal evaporation of Aluminum through a mask. The piezoelectric properties of the BAW transducer are deduced from the electrical input impedance measured by a HP8753ES Network Analyzer in the harmonic regime.

4. Piezoelectric characterization of the device

The representation of the electrical input impedance in Fig.6 shows some resonance peaks located at frequencies which are multiples of the fundamental mode frequency. It shows also some parasitic modes (denoted by PM). The fundamental resonance in thickness mode vibration is observed at f_r=157.4 MHz and the anti-resonance frequency appears at f_a=159.5 MHz. The electrical resistance at resonance is 10.5 Ω, whereas, at the anti-resonance, it becomes equal to 186.2 Ω. For each mode taken separately, the phase representation (dashed line) shows that the resonator behaves like a capacitance (*Phase(Z)=-π/2*) just before resonance. It switches to an inductive behavior between the resonance and the anti-resonance. Then, it becomes again capacitive after the anti-resonance frequency [26].

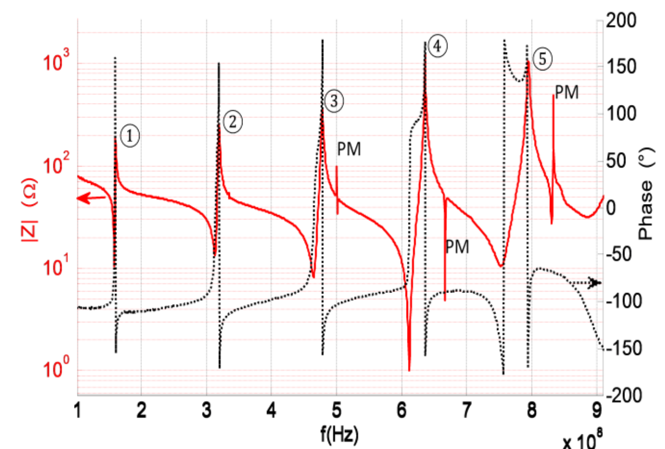

Fig. 6: Electrical input impedance (magnitude and phase) of the BAW device.

The effective electromechanical coupling coefficient [27], K_{eff}, is related to the resonance and the anti-resonance frequencies by the equation (3):

$$K_{eff}^2 = \frac{\pi f_r}{2 f_a} . \tan^{-1}(\frac{\pi f_r}{2 f_a}) \quad (2)$$

The previous values of f_r and f_a corresponding to the first mode (fundamental mode) lead to K_{eff}^2=3.21 %. The table(1) shows the results for the fundamental mode and for the higher order harmonics.

Table 1 : Characteristics of the resonance peaks.

Mode	f_r (MHz)	f_a (MHz)	R_r(Ω)	R_a(Ω)	K_{eff}^2(%)
1st mode (fundamental)	157.4	159.5	10.5	186.2	3.21
2nd mode	312.5	318.8	13.4	260.3	4.78
3rd mode	464.4	478.1	8.3	370.7	6.87
4th mode	611.86	636.26	1	1258	9.10

The best electromechanical coupling coefficient is obtained for the fourth (4th) mode, with K_{eff}^2=9.10 %, where the electrical resistance at the resonance frequency shows the smallest value (R_r=1 Ω), and the resistance at the anti-resonance frequency exhibits the largest value (R_a=1.26 kΩ).

5. Conclusion

The piezoelectric ZnO layer was prepared by the PLD technique at different substrate temperatures, from 100 to 500°C. The XRD measurements showed that the deposited ZnO films were *c*-axis (002) oriented, corresponding to the wurtzite structure, and indicated that 300°C was the optimal substrate temperature to obtain the well crystallized ZnO on Al buffer layer. The SEM characterization showed the evidence of a columnar structure on the cross-section, which was perpendicular to the substrate surface, it also showed an evidence of compact grains on the surface forming a honeycomb-like structure. The good crystallinity and mosaicity of the ZnO film are confirmed by the low value of the rocking curve FWHM measurement.

The elaborated ZnO layer is used in Al/ZnO/Al/SiO_2/Si BAW resonator, the device can work at a frequency which is a multiple of the fundamental mode frequency (157.4 MHz), but the best working frequency corresponds to the fourth harmonic and is located at 611.86 MHz. Indeed, at this frequency, the device presents simultaneously the highest piezoelectric performances with the largest piezoelectric coupling coefficient (K_{eff}^2=9.1%), the smallest electrical resistance at the resonance frequency and the largest electrical resistance at the anti-resonance frequency.

Acknowledgment

The authors wish to express their gratitude to Mr. F. Metehri for his help in the clean room. They would like to acknowledge all the MEMS team of the CDTA center, especially Mr. H. Khales and Mr. W. Aouimeur for their help in the electrical characterization.

References

[1] J.C. Fan, K.M. Sreekanth, Z. Xie, S.L. Chang and K.V. Rao, p-Type ZnO materials: Theory, growth, properties and devices, Progress in Materials Science, 58 (2013) 874–985.
[2] H.S. Al-Salman and M. J. Abdullah, Hydrogen Sensing Based on ZnO Nanostructures Prepared by RF-Sputtering on Thermally Oxidized Porous Silicon, Sensor Letters, 01/2015; 13(1).
[3] M. Benhaliliba, Y.S. Ocak, H. Mokhtari, C.E. Benouis, M.S. Aida. The microelectronic parameters of Al /ZnO/p-Si/Al Schottky diode for solar cell applications, DUFED 4(1) (2015) 1-3).
[4] T. Gryba, J. Carlier, S. Wang, X.Z. Zhao, S. Guo and J.-E. Lefebvre, One port contour-mode ZnO piezoelectric MEMS resonator, Microelectronic Engineering, 88 (2011) 3003–3010.
[5] B.P. Nabar1, Z. Çelik-Butlern and D.P. Butler, Piezoelectric ZnO nanorod carpet as a NEMS vibrational energy harvester, Nano Energy, 10 (2014) 71-82.
[6] S. Joshi, M. Parmar and K. Rajanna, A novel gas flow sensing application using piezoelectric ZnO thin films deposited on Phynox alloy, Sens. and Actuators A, 187 (2012) 194–200.
[7] A.J. Festschrift, J. Luo, Y.Q. Fu, L. Garcia-Gancedo, X.Y. Du, J.R. Lu, X. B. Zhao, E. Iborra, M. Ramos, and W. Milne, *ZnO based SAW and FBAR devices for bio-sensing applications.* Journal of Non-Newtonian Fluid Mechanics, 222 (2015) 209-216.
[8] X. Bian, H. Jin, X. Wang, S. Dong, G. Chen, J.K. Luo, M. Jamal Deen, and B. Qi, UV sensing using film bulk acoustic resonators based on Au/n-ZnO/piezoelectric-ZnO/Al structure, Sci Rep., 5 (2015) 9123.
[9] H.L. Ma, Z.W. Liu, D.C. Zeng, M.L. Zhong, H.Y. Yu, and E. Mikmekova, Nanostructured ZnO films with various morphologies prepared by ultrasonic spray pyrolysis and its growing process, Applied Surface Science, 283 (2013) 1006-1011.
[10] L.W. Wang, F. Wu, D.X. Tian, W.J. Li, L. Fang, C.Y. Kong and M. Zhou, Effect of Na content on structural and optical properties of Na-doped ZnO thin films prepared by sol-gel method, J. Alloys Comp., 623 (2015) 367-373.
[11] H.S. Al-Salman and M.J. Abdullah, Preparation of ZnO nanostructure by RF-magnetron sputtering on thermally oxidized porous silicon substrate for VOC sensing application, Measurement, 59 (2015) 248-257.
[12] M. Acuautla, S. Bernardini, L. Gallais, T. Fiorido, L. Patout, M. Bendahan,Ozone flexible sensors fabricated by photolithography and laser ablation

processes based on ZnO nanoparticales, Sens. Actuators B 203 (2014) 602-611.

[13] S.S. Xiao, L. Zhao, Y.H. Liu and J.S. Lian, Nanocrystalline ZnO films prepared by pulsed laser deposition and their abnormal optical properties, Applied Surface Science 283 (2013) 781– 787

[14] K. Bdikin, J. Gracio, R. Ayouchi, R. Schwarz and A.L. Kholkin, Local piezoelectric properties of ZnO thin films prepared by RF-Plasma-assisted pulsed-laser deposition method, Nanotechnology 21 (2010) 235703 (6pp).

[15] R. Serhane, S. Abdelli-Messaci, S. Lafane, H. Khales, W. Aouimeur, A. Hassein-Bey and T. Boutkedjirt, Pulsed Laser Deposition of Piezoelectric ZnO Thin Films Bulk Acoustic Wave Devices, Applied Surface Science, 288 (2014) 572-578.

[16] J. Goulon, N. Jaouen, A. Rogalev, F. Wilhelm, C. Goulon-Ginet, C. Brouder, Y. Joly, E.N Ovchinnikova, and V.E Dmitrienko, Vector part of optical activity probed with x-rays in hexagonal ZnO, J. Phys. Condens. Matter. 19 (2007) 156201.

[17] B.D. Cullity, Element of X-ray Diffraction, 2nd ed., Addison-Wesley Pub Co, Boston, MA, 1978.

[18] S.L. King, J.G.E. Gardeniers and I.W. Boyd, Pulsed-laser deposited ZnO for device applications, Applied Surface Science, 96-98 (1996) 811-818.

[19] Y. Yoshino, M. Takeuchi, K. Inoue, T. Makino, S. Arai and T. Hata, Control of temperature coefficient of frequency in zinc oxide thin film bulk acoustic wave resonators at various frequency ranges, Vacuum, 66 (2002) 467-472.

[20] E. A. Irene, Electronic Materials Science, Wiley, New Jersey, 2005, p.22.

[21] E.H. Kisi and M.M. Elcombe, u parameters for the wurtzite structure of ZnS and ZnO using powder neutron diffraction, Acta Cristallographica C, 45 (1989) 1867-1870.

[22] M. Nistor, N.B. Mandache, J. Perrière, C. Hebert, F. Gherendi and W. Seiler, Growth, structural and electrical properties of polar ZnO thin films on MgO (100) substrates, Thin Solid Films 519 (2011) 3959-3964.

[23] J. Perrière, E. Millon, and V. Craciun, ZnO and ZnO-Related Compounds, in : Robert Eason (Eds), Pulsed Laser Deposition of Thin Films: Application Led Growth of functional Materials, John Wiley & Sons, 2007. pp.261-289.

[24] S.J. Pearton, D.P. Norton, K. Ip, Y.W. Heo, and T. Steiner, Recent progress in processing and properties of ZnO, Prog. Mater. Sci., 50 (2005) 293-340.

[25] M.C. Tamargo, II-VI Semiconductor materials and their applications, Volume.12, Taylor & Francis (2001).

[26] R. Serhane, T. Boutkedjirt, and A. Hassein-Bey, in IEEE Explorer of the 24th International Conference on Microelectronics (Algiers, 2012).

[27] S.R. Naik, J.J. Lutsky, R. Reif and C.G. Sodini, Electromechanical Coupling Constant Extraction of Thin-Film Piezoelectric Materials using a Bulk Acoustic Wave Resonator, IEEE UFFC, N°.1, 45 (1998) 257-263.